Electrospun Microfiber Membranes Embedded with Drug-Loaded Clay Nanotubes for Sustained Antimicrobial Protection

Jiajia Xue,[†,‡] Yuzhao Niu,[†] Min Gong,[‡] Rui Shi,[∥] Dafu Chen,[∥] Liqun Zhang,[*,†,‡] and Yuri Lvov[*,§]

[†]Beijing Laboratory of Biomedical Materials and [‡]State Key Laboratory of Organic—Inorganic Composites, Beijing University of Chemical Technology, Beijing 100029, PR China, [§]Biomedical Engineering Program, Louisiana Tech University, Ruston, Louisiana 71270, United States, and [∥]Laboratory of Bone Tissue Engineering of Beijing Research Institute of Traumatology and Orthopaedics, Beijing 100035, PR China

ABSTRACT Guided tissue regeneration/guided bone regeneration membranes with sustained drug delivery were developed by electrospinning drug-loaded halloysite clay nanotubes doped into poly(caprolactone)/gelatin microfibers. Use of 20 wt % nanotube content in fiber membranes allowed for 25 wt % metronidazole drug loading in the membrane. Nanotubes with a diameter of 50 nm and a length of 600 nm were aligned within the 400 nm diameter electrospun fibers, resulting in membranes with doubling of tensile strength along the collector rotating direction. The halloysite-doped membranes acted as barriers against cell ingrows and have good biocompatibility. The metronidazole-loaded halloysite nanotubes incorporated in the microfibers allowed for extended release of the drugs over 20 days, compared to 4 days when directly admixed into the microfibers. The sustained release of metronidazole from the membranes prevented the colonization of anaerobic Fusobacteria, while eukaryotic cells could still adhere to and proliferate on the drug-loaded composite membranes. This indicates the potential of halloysite clay nanotubes as drug containers that can be incorporated into electrospun membranes for clinical applications.

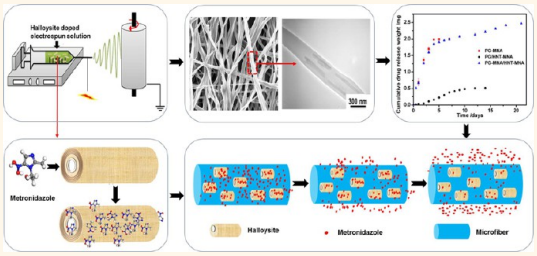

KEYWORDS: guided tissue regeneration · anti-infection · electrospinning · clay nanotubes · sustained drug delivery

Guided tissue regeneration/guided bone regeneration (GTR/GBR) technologies are becoming a standard approach for tissue and bone therapy.[1] GTR/GBR membranes are used not only to perform the barrier function preventing the ingrowth of fibroblast cells into the defective tissue but also to improve the regeneration rate by supporting attachment and proliferation of cells.[2] Development of biodegradable GTR/GBR membranes with flexibility, adequate mechanical properties, biocompatibility, and a proper degradation profile will eliminate the need for membrane removal surgery.[3]

Tissue trauma and invasive surgery, which is required for GTR/GBR, can cause infection which may lead to implant failure, constituting a significant healthcare burden.[4] The most common cause of infection is bacterial colonization at the wound site. The implant can also fail, or be rejected, due to the foreign body response resulting from implant material. The foreign body response can be avoided by improving the biocompatibility of the material, while bacterial infections can be managed by antibacterial drugs.[5] Controlled local delivery of antibacterial drugs to the infection site at a minimal inhibitory concentration is desired to avoid the systemic toxicity with conventional administration.[6] Thus, GTR/GBR membrane with high biocompatibility and with local delivery of antibiotics that can be sustained for at least 2 weeks is critical in decreasing postsurgery infection, which is mainly caused by anaerobic bacteria.[7] Metronidazole (MNA), which has selective activity against anaerobic microorganisms, has been used for the treatment of bacterial infections.[8]

The technique of electrospinning membranes has seen a rise in interest as a method

* Address correspondence to zhanglq@mail.buct.edu.cn, ylvov@latech.edu.

Received for review November 2, 2014 and accepted January 13, 2015.

Published online January 13, 2015
10.1021/nn506255e

of polymer-fiber processing for applications in tissue engineering with drug release.[9] The micronano scale organization and high porosity of electrospun membranes, which is similar to the natural extracellular matrix, is favorable for adhesion and proliferation of cells and decreases the immune response.[10] In addition, controlled local drug delivery can be realized by electrospun fibers. Previously, we developed an efficient GTR/GBR implant made from metronidazole-loaded electrospun polycaprolactone/gelatin which reduced the inflammatory response in rabbits by delivering metronidazole locally.[11] A polycaprolactone/gelatin of 80:20 ratio was found to be optimal for biodegradation. However, the release time of metronidazole was only few days. An extended drug release profile is necessary for severe postsurgery infections.[12] The drug release profile can be adjusted by the utilizing the proper nanoarchitecture of electrospun microfibers, for example, with the inclusion of drug-loaded nanotubes.

The "nano in micro" composite is a promising architectural approach for the design of a sustained drug delivery vehicle that combines the drug-loading capability of nanoparticles or nanotubes and electrospinning technology.[13−15] Encapsulation of antibiotics, particularly within nanoscale containers, has the potential for prolonged release. Halloysite clay nanotubes are one such type of container.[15−17] Halloysite is a tubule aluminosilicate clay with an external diameter of 50−60 nm, lumen diameter of 12−15 nm, and a length of 600−700 nm. Halloysite is a cheap and natural material that is produced in amounts of thousands of tons.[17,18] It has excellent biocompatibility, which has been assessed for both cell cultures and animal tissues.[19,20] Various kinds of drugs can be loaded in halloysite nanotubes (HNTs).[21] By embedding the drug-loaded clay nanotubes inside of the electrospun microfibers, the sustained release of the drug was observed.[22] The typical release time of an antibiotic from halloysite in water is 10−20 h (*e.g.*, gentamicin, ciprofloxacin, tetracycline). After these tubes were embedded in a polymeric matrix, clogging at the end of the tubes increased release to 2−3 weeks.[16,21−23]

The mechanical properties of the electrospun fiber membranes can also be improved by the incorporation of inorganic nanotubule materials. Assuming that the drug is not toxic, higher and longer lasting drug concentration at the surgery site gives a stronger therapeutic effect. Therefore, our purpose is to develop a drug-loaded halloysite/electrospun nanomicro composite fiber membrane with prolonged drug release and high therapeutic drug content as an anti-infective GTR/GBR membrane. The current study aimed to (i) investigate the influence of halloysite nanotube inclusion on the properties of electrospun microfiber membranes and (ii) develop antibacterial membranes

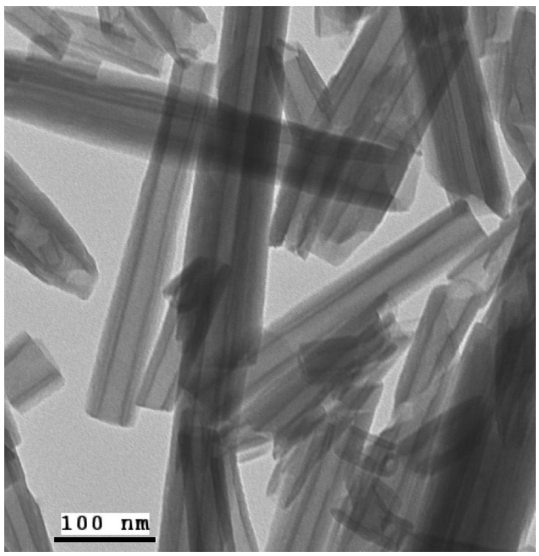

Figure 1. TEM image of halloysite nanotubes.

with longer drug release profiles of 3 weeks. The solvent used for electrospinning polycaprolactone−gelatin mixtures is trifluoroethanol, in which halloysite aggregates. It was necessary to modify the tubes with (aminopropyl)triethoxysilane (APTES) to resolve this issue. Next, metronidazole-loaded nanotubes were mixed with the polymeric solution for electrospinning to form a composite fiber membrane. The properties of the membranes were optimized for long-lasting release of antibiotics with improved mechanical strength and biocompatibility. This approach is based on unique architectural design of microfibers with tubular nanocontainers which may be extended for different drugs or cocktails of drugs that can fight antibiotic resistant species.

RESULTS AND DISCUSSION

Halloysite clay is an abundantly available nanotube formed by rolled kaolin sheets, and its chemical formula in dried form is $Al_2O_3 \cdot 2SiO_2 \cdot 2H_2O$. Halloysite tubes have a diameter of 50 ± 10 nm with an inner lumen diameter of 15 ± 5 nm. The length distribution of halloysite tubes obeys Gaussian law with overage 720 nm and the distribution width of 270 nm (Figure 1). The nanotube wall contains ca. 15 densely packed alumosilicate sheets with spacing of 0.72 nm, and its density is 2.53 g/cm^3. The surface of halloysite tubes is silica, and the lumen is alumina. The measured ξ-potential of the surface and lumen are −30 and +25 mV, respectively, at moderate pH. It is this position of charge which allows the tube to contain negatively charged molecules inside of the lumen.[16,17]

The strategy for the development of halloysite nanocontainers includes (1) modification of the surface of the tubes in order to improve dispersion in trifluoroethanol; (2) production of polycaprolactone−gelatin microfibers with a diameter less than the length of the

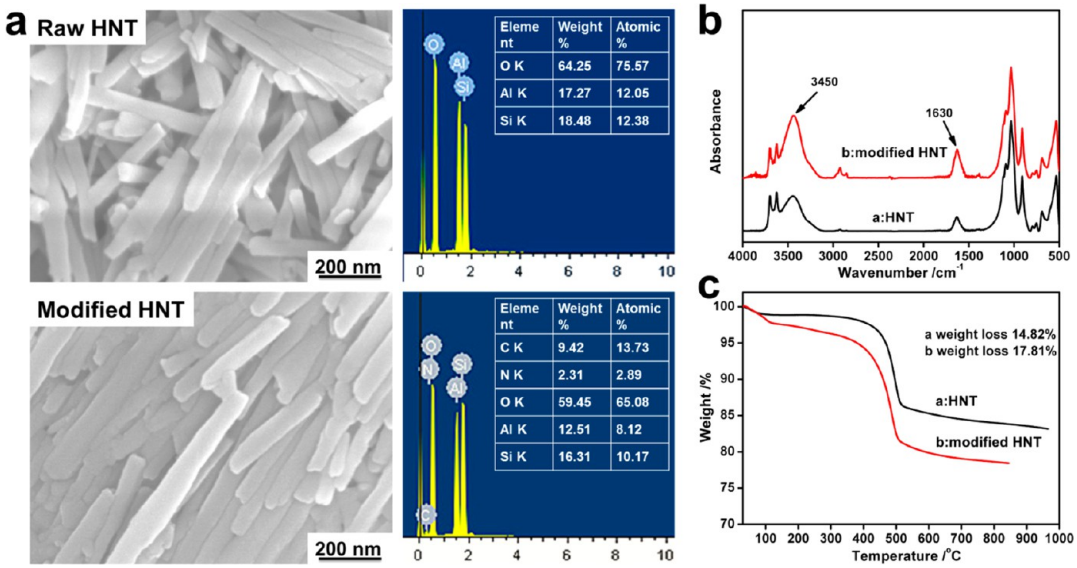

Figure 2. Characterization of HNT before and after modification with silane coupling: (a) SEM images and EDX spectra, (b) FT-IR spectra, and (c) TGA curves.

nanotubes (this is necessary to induce their orientation through spatial confinement and maximization of the tube's content without fiber distortion, and improving mechanical properties of such composite electrospun material); (3) determination of biocompatibility and biodegradation of the membranes; (4) optimization of drug loading and release with halloysite nanotube microfiber membranes, extending the drug release time for the nano- composite tissue; and (5) increasing the antimicrobial efficiency for 2−3 weeks postsurgery recovery period.

1. Surface Modification of Halloysite Nanotubes. The surface of the nanotubes was silanized with aminopropyltriethoxysilane (APTES) to improve their dispersivity in the electrospinning solvent. SEM−EDX elemental analysis revealed the presence of carbon and nitrogen atoms on the modified surface of the HNTs, which is indicative of the APTES coating (Figure 2a). The silanization did not change the tubular structure of the halloysite. The FTIR spectra before and after modification are given in Figure 2b. The spectrum of pristine halloysite showed two Al_2OH stretching absorption bands at 3699 and 3628 cm^{-1}, each OH being linked to two Al atoms, in-plane Si−O−Si stretching (1095 and 1032 cm^{-1}), and a single Al_2OH bending band at 910 cm^{-1}.[24,25] The intensity of the absorption peak at 3450 cm^{-1} (NH_2 stretching vibration) and 1630 cm^{-1} (NH_2 inplane bending vibration) of the modified HNT increased compared with the pristine one, indicating that the silane coupling was successfully grafted.[24] Thermogravimetric analysis (TGA) of halloysite (Figure 2c) before and after modification revealed a weight loss of 14.8 wt % in the 100 to 550 °C range due to structural dehydoxylation, while for modified HNT the weight loss was 17.8 wt % within the same temperature range. The difference of 3.0 wt % may be attributed to decomposition of the grafted silane.[25] Taking into account the nanotube diameter and the densities of both halloysite and APTES, one can calculate a surface coating thickness of 0.8 ± 0.2 nm which indicates successful tube modification. After this treatment, uniform dispersions of halloysite in trifluoroethanol were stable for over 2 weeks.

The MTT method was used to check whether the modification procedure influenced the cytotoxicity of halloysite. The morphologies of L929 mouse cells, which had been incubated for 72 h with different HNT concentrations, showed spindle, triangular, and quadrangular shapes with good growing conditions confirming the cells' viability and nanotube biocompatibility (Figure S1, Supporting Information).

2. Characterization of the Nanotube-Doped Microfiber Membranes. Different amounts of halloysite were added into the microfibers to determine the highest tube content that could be doped. The polycaprolactone−gelatin membranes with the nanotube contents of 0, 1, 2, 5, 10, and 20 wt % relative to the polymer mass were labeled as HNT0, HNT1, HNT2, HNT5, HNT10, and HNT20. The membranes show a randomly interconnected structure with no beads formed and uniform distribution of the fibers (Figure 3). The incorporation of halloysite does not significantly influence the morphology of the fibers and tissue even when its content reached 20 wt % (which corresponds to 8 vol %). The diameters of the fibers are in submicron range of 300−500 nm (Table 1). The 1.1−1.7 μm pore size of the membranes is much smaller than the size of fibroblast cells (about 20 μm), thus providing membrane barrier to prevent the ingrowth of fibroblasts into the tissue defects.

TEM images show halloysite tubes orientation along the fiber direction (Figure 4). With the increase

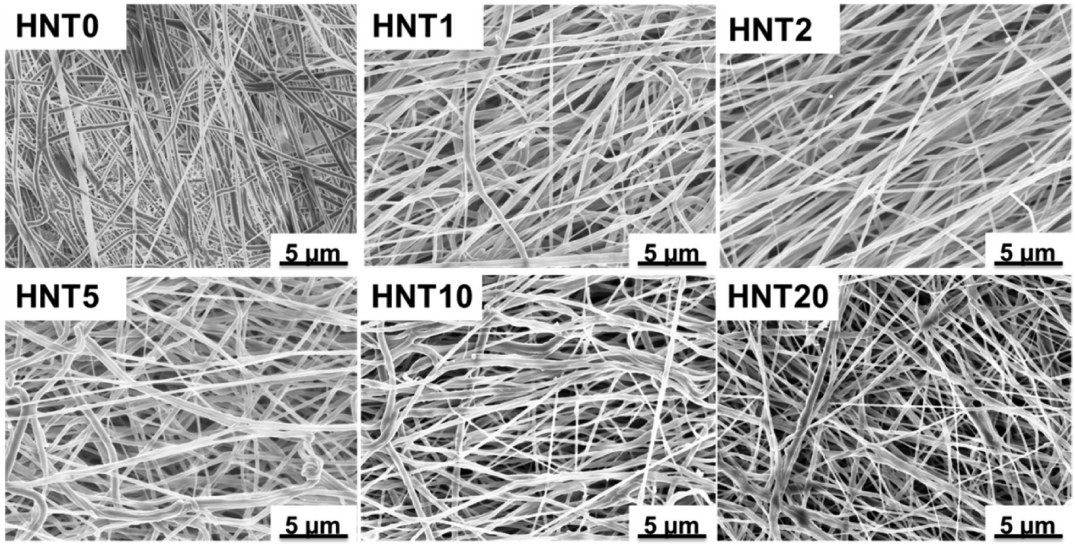

Figure 3. SEM micrographs of the electrospun halloysite doped microfiber membranes with different contents of HNT (0, 1, 2, 5, 10, and 20 wt %).

TABLE 1. Fiber Diameter and Pore Size of the Electrospun HNT-Doped Microfiber Membranes with Different Contents of Nanotubes

sample	fiber diameter (μm)	pore size (μm)
HNT0	0.48 ± 0.15	1.16 ± 0.76
HNT1	0.32 ± 0.16	1.21 ± 1.92
HNT2	0.35 ± 0.13	1.47 ± 0.80
HNT5	0.37 ± 0.13	1.49 ± 0.64
HNT10	0.39 ± 0.20	1.56 ± 0.87
HNT20	0.48 ± 0.14	1.74 ± 0.71

of halloysite content in the initial dispersion, the tube amount in the fibers proportionally increases. Due to silanization of halloysite surface, the nanotubes were well dispersed in the electrospinning polymeric solution resulting in the homogeneous distribution of HNT in the microfibers. This alignment of HNT in the fibers provides the nanomicro composite membrane with anisotropic mechanical properties, and the drug release kinetics may be controlled by the nanotube's openings clogged with the fiber polymers.

The influence of halloysite on the thermal and chemical properties of the composite fiber membranes are presented in Figure 5. According to the thermogravimetric (TGA) profiles, all electrospun fiber membranes decompose in a single step at ca. 405 °C. The onset decomposition temperature increases with the tube content, indicating that halloysite improves thermal stability of the membranes. Besides, the increased residual weight of the membranes with the halloysite content corresponds to the incorporation rate of the nanotubes into the fibers.

The inclusion of halloysite had no significant influence on the crystallinity of polycaprolactone as follows from the differential scanning calorimetry (DSC) thermograms (Figure 5b). The melting ranges of polycaprolactone is broadening with the halloysite content, indicating the presence of different size crystals in the fibers. Halloysite may act as a crystallization nucleation sites, changing and restricting the polymer crystallinity. A similar effect was found for halloysite–polypropylene composites.[17]

In Fourier transform infrared (FT-IR) spectra of the electrospun membranes (Figure 5c), the characteristic peaks of gelatin appear at 1650 cm^{-1} (amide I) and 1540 cm^{-1} (amide II). The PCL-related stretching modes are represented by the peaks at 2943 cm^{-1} (asymmetric CH_2 stretching), 2866 cm^{-1} (symmetric CH_2 stretching), 1721 cm^{-1} (C═O stretching), 1294 cm^{-1} (C–O and C–C stretching), and 1240 cm^{-1} (asymmetric C–O–C stretching).[26] The incorporation of halloysite had no significant influence on the chemical composition of the polymer matrix.

In the X-ray diffraction (XRD) patterns (Figure 5d), two diffraction peaks located at scattering angles of 21.4° and 23.8° are assigned to semicrystalline polycaprolactone, and amorphous gelatin does not give Bragg reflections. The intensity of the diffraction peaks decreases with the increase of halloysite content, which is consistent with the DSC results, indicating that the nanotubes restrain crystallization of polycaprolactone. At low halloysite content, its characteristic diffraction peaks are not detectable. As the halloysite content exceeds 5 wt %, the signal accumulates and the clay multiwall packing peak appears at 12.4° corresponding to 0.72 nm, also proving an incorporation of halloysite into the microfibers.

For bone/tissue regeneration, the porous membrane must be strong enough to withstand the stresses during the surgical procedure. The mechanical properties of a membrane depend on the microstructure of each individual fiber, and, on a large scale,

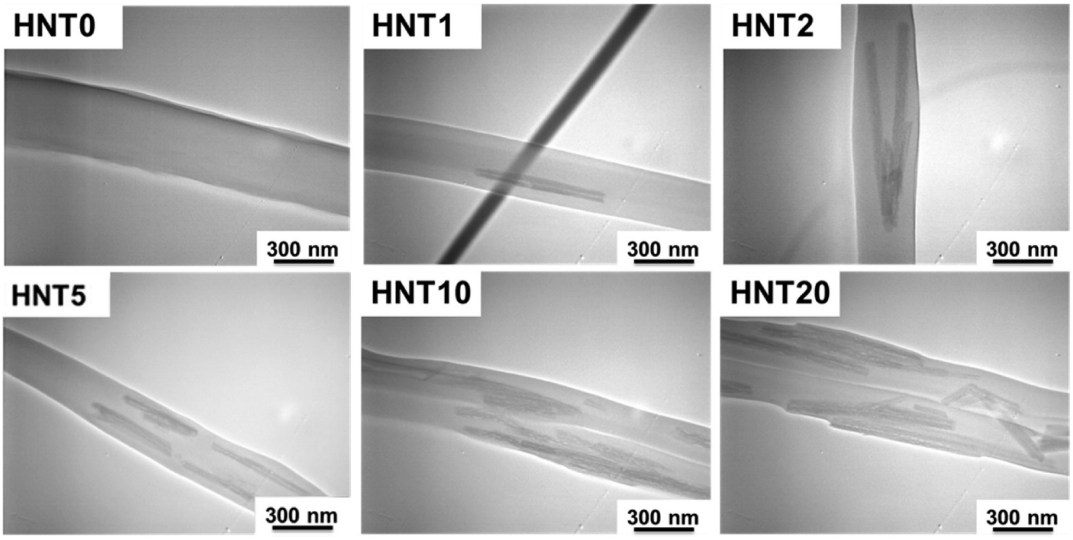

Figure 4. TEM micrographs of the halloysite doped microfibers with different tube contents.

on the membrane porosity, the presence and density of bonding sites between the micorfibers, and their alignment.[27] For example, nanohydroxyapatite/polyamide guided tissue regeneration (GTR) membranes had tensile strengths of 2−3 MPa, which already satisfied the GTR requirements.[28] The membrane works in a body fluid environment (it needs to be soaked in saline before implant surgery), and its mechanical properties were characterized in the wet state.

The mechanical properties of the wet membranes at directions along and perpendicular to the collector rotating direction were evaluated (Figure 5e,f and Table 2), and the last point in the stress−strain curve means tensile strength of the membranes. The tensile strength of the membranes is in the range of 3.0−7.3 MPa (depending on halloysite concentration) in the perpendicular direction while it is 7.4−15.3 MPa along the collector rotating direction, showing an anisotropic mechanical properties. In no-halloysite, pure polymeric membrane, tensile strength in any direction is 7.3−7.6 MPa. So, the strength of the nanomicro composite halloysite membranes along the collector rotation direction is two times higher than the one in the perpendicular direction. During the electrospinning process, the nanotubes are aligned in the microfibers, and these composite fibers were predominantly oriented along the collector rotation direction. With more halloysite, the longitudal tensile strength increased, probably because the nanotubes could bridge the microfibers. The stress−strain curves show that the membranes are elastic in both directions (a property critical for GTR membranes), and their tensile strength >3 MPa is high enough to meet the clinical requirements. This HNT-doped composite microfiber membrane with anisotropic mechanical properties may beneficial for the regeneration because native tissues and organs often have anisotropy.

3. Biocompatibility and Biodegradation of the Membranes. The hydrophilicity of the membrane, which can be tailored by its composition, has great influence on the adhesion and proliferation of cells.[29,30] The water droplets on the surface of the electrospun membranes are shown in Figure 6. For no halloysite sample, the membrane shows hydrophobic surface. With the increase of halloysite content, the HNT-fiber membranes become more hydrophilic with the decrease of contact angles from ca. 105 to 80°. The contact angles decreased with time because of the water absorption property of the membranes. Water is completely absorbed within 5 s for HNT10 and HNT20 samples. Incorporation of halloysite significantly increases the hydrophilicity of the membranes and this improves tissue regeneration and the biodegradation rate.

A desirable feature of implantable scaffolds is synchronization of polymer membrane degradation with the replacement by natural tissue. The GTR membranes must function for 4−5 weeks to allow regeneration of the periodontal system.[31] Our membranes show mass loss in 2 weeks caused by gelatin hydrolysis on the surface of the microfibers followed with slow and linear degradation rate with hydrolysis of gelatin (Figure S2, Supporting Information). The incorporation of halloysite increases the biodegradation rate, probably due to increased hydrophilicity. SEM micrographs of the membranes after 15 days of degradation indicate that the morphology of the fibers was not changed and the membrane is still strong enough for new tissue regeneration. The barrier function of the halloysite nanomicro fiber membranes was tested *in vitro* by penetration of fibroblast cells. No cell protrudes to the opposite side of the membranes (Figure S3, Supporting Information).

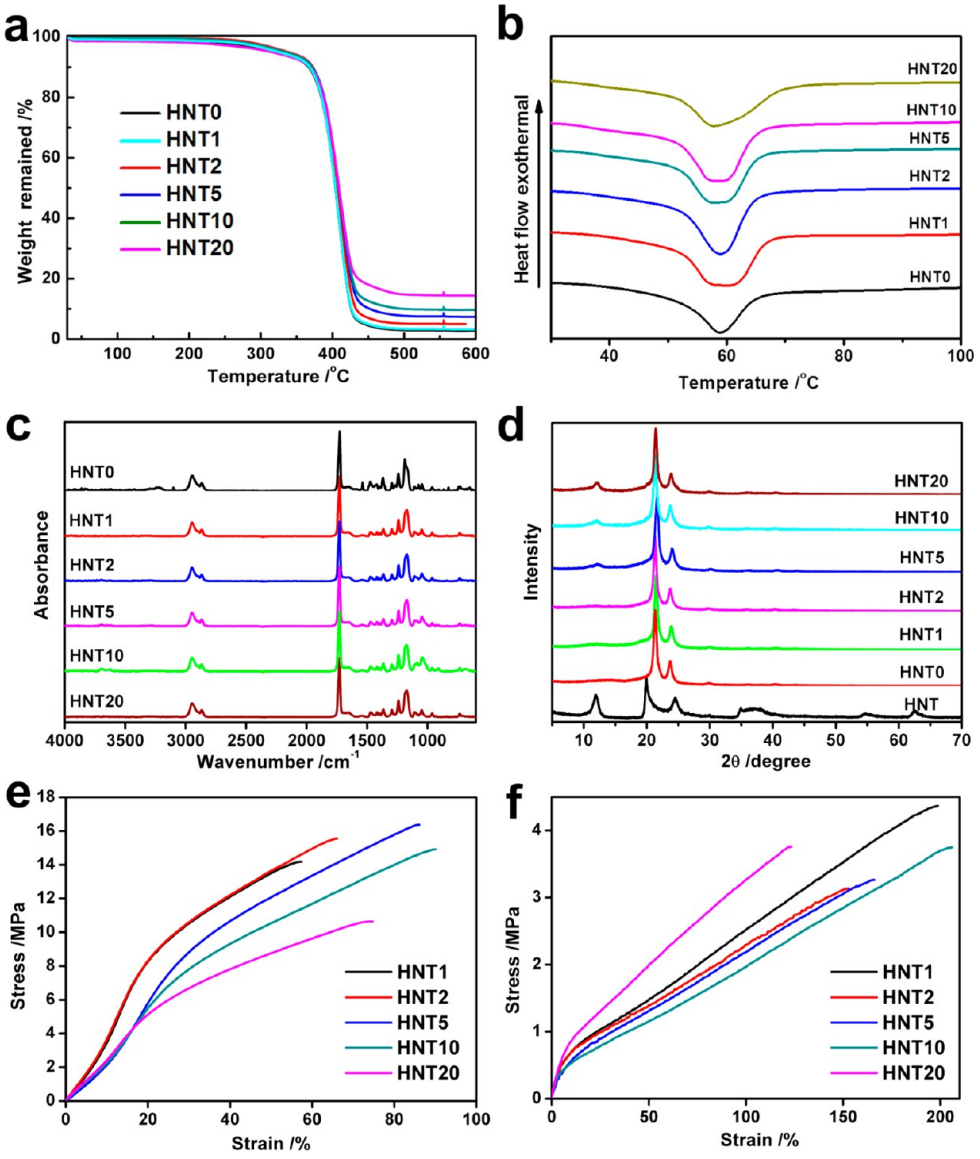

Figure 5. Thermal, structural, and mechanical characteristics of the electrospun halloysite doped microfiber membranes with different contents of HNT (0, 1, 2, 5, 10, and 20 wt %): (a) TGA profiles, (b) DSC thermograms, (c) FTIR spectra, (d) XRD patterns, and stress−strain curves in the wet state at different directions (e) along the collector rotating direction and (f) perpendicular to the collector rotating direction.

TABLE 2. Mechanical Properties of the Wet Electrospun Halloysite Doped Microfiber Membranes with Different Contents of HNT at Directions along and Perpendicular to the Collector Rotating

	along the collector rotating direction		perpendicular to the collector rotating direction	
sample	tensile Strength (MPa)	elongation at break (%)	tensile strength (MPa)	elongation at break (%)
HNT0	7.6 ± 1.1	127.0 ± 4.7	7.3 ± 0.3	72.7 ± 13.3
HNT1	15.3 ± 2.2	74.4 ± 11.3	4.4 ± 0.1	205.4 ± 3.9
HNT2	15.8 ± 0.5	71.1 ± 7.3	3.0 ± 0.3	150.1 ± 13.3
HNT5	16.0 ± 0.9	85.4 ± 13.3	3.2 ± 0.2	169.7 ± 4.6
HNT10	14.8 ± 0.3	92.7 ± 7.9	3.0 ± 0.5	211.4 ± 1.2
HNT20	7.4 ± 0.4	61.1 ± 10.3	4.1 ± 0.7	137.1 ± 19.3

From the *in vitro* results (Figure 7), the HNT−microfiber membranes with different nanotube contents show no cytotoxicity to L929 mouse cells. Incubated in the extract of the membranes, L929 cells show healthy-growth morphologies. Attachment, adhesion, and spreading occur in the first phase of cell−material interactions and improve the cell's capacity to proliferate.

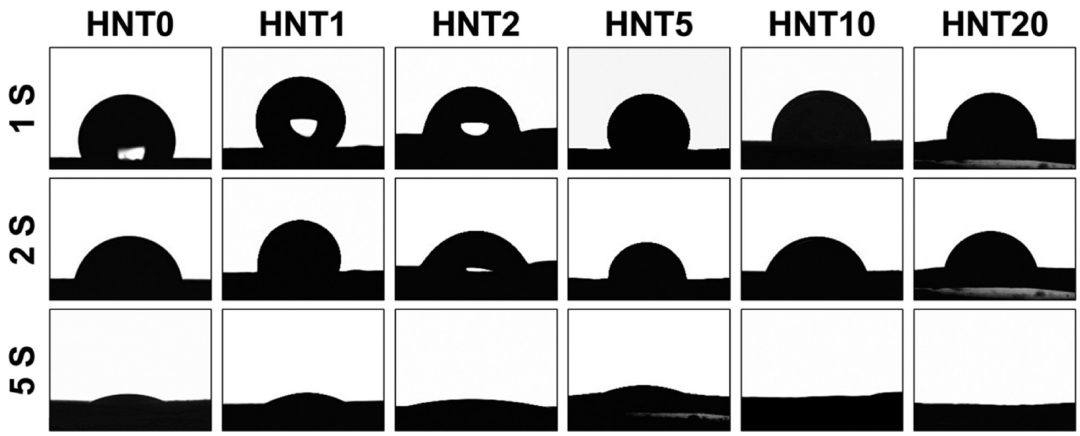

Figure 6. Wetting behavior of a water droplet on the surface of the electrospun halloysite membranes with different contents of HNT (0, 1, 2, 5, 10, and 20 wt %).

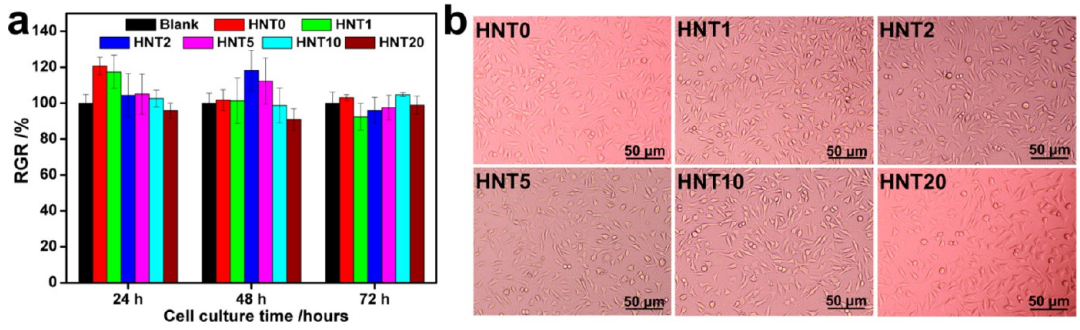

Figure 7. Results of the *in vitro* cytotoxicity: (a) O.D. of L929 cells cultured for 24, 48, and 72 h and (b) microscope images of L929 cells cultured for 24 h in extract substrates of the of the electrospun HNT doped microfiber membranes.

The morphology of L929 cells proliferating 5 days on the membranes was observed by SEM and CLSM (Figure 8). The cells grow on the membrane without infiltrating in the depth because of the small membrane pores. L929 cells reach approximately 50−60% confluency with both stretching spindle shapes. The specific structures related to the cell motility of fibroblasts, filopodia and lamellipodia, can be observed. The elongated cell filopodia extensions toward the fibers and neighboring cells can bridge and communicate with the surrounding microenvironment and neighboring cells.[32] The optical density of L929 cells adhered to TCP (the control substrate) and the membranes, 4 h after being seeded, are shown in Figure 8n. There are no significant differences between the membranes with different halloysite content and control: cells adhere well onto all tested substrates. With incubation, the number of cells increases continuously during 7 days, indicating that the nanomicro composites are nontoxic and support cells' proliferation. The highest 20 wt % of halloysite doped into the membranes has no cytotoxicity while maximizing drug load which promises the best antibacterial activity.

4. Drug Loading and Release with Halloysite Microfiber Membranes. The loading content of metronidazole (MNA) in halloysite nanotubes is affected by the solvent, drug concentration and the drug/HNT mass ratio. Metronidazole was dissolved in methanol at 100 mg/mL, and surface modified halloysite was also dispersed well in the methanol drug solutions. The mass ratio of MNA:HNT was chosen as 4:1 for the highest drug-loading efficiency. The final metronidazole loading content was 25 wt %, which meant that metronidazole molecules were not only encapsulated inside the tube (which lumen is ca. 10 vol %) but also absorbed in the external pockets and on the tube surface.

The release of the drug incorporated into halloysite was first studied in trifluoroethanol under magnetic stirring. Metronidazole was released from the nanotubes in 25 h (Figure S4, Supporting Information): a rapid release of 70% MNA in the first 10 h followed by slower release and may be well fitted with Peppas model[33] ($M_t/M_\infty = kt^n$, where M_t is the amount of drug released at time t, M_∞ is the amount of drug released at infinite time, k is a constant, and $n = 0.4$ is the exponent characteristic of the release mechanism). These are not actual nanomicro fiber release conditions and characterizes only the nanotubes loading.

Next, we incorporated loaded nanotubes into electrospun microfiber membrane which resulted in much slower drug release kinetics. For no-halloysite electrospun membranes, 30 wt % metronidazole (MNA) content is the highest drug content without cytotoxicity.[11] So, in this study, the whole drug content incorporated

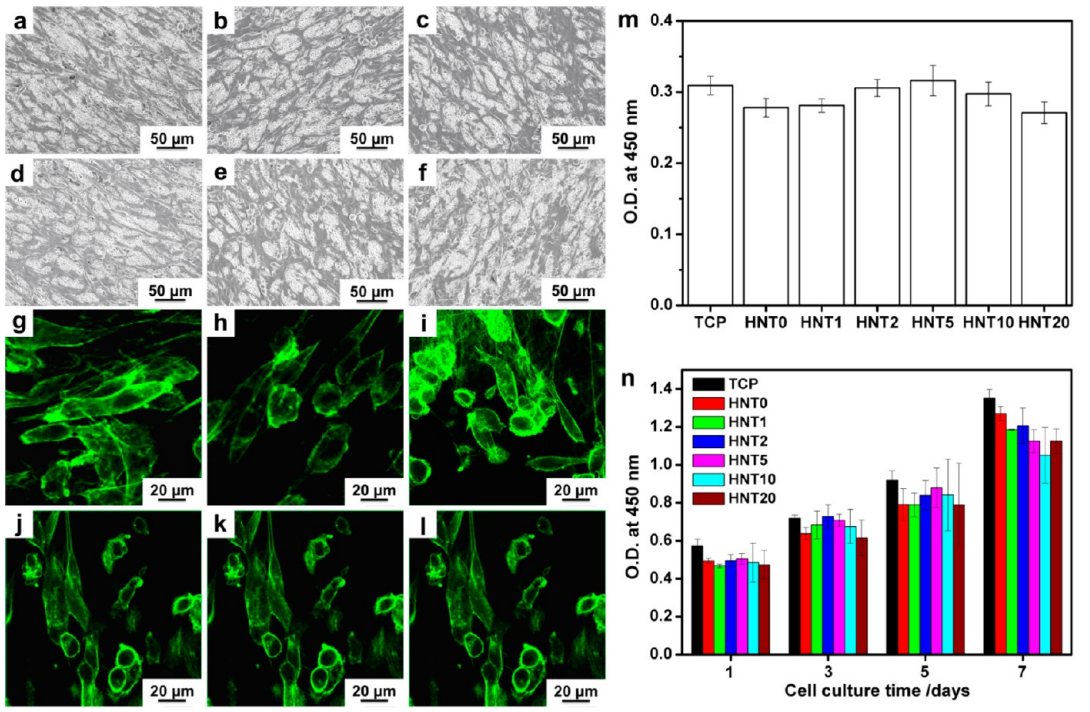

Figure 8. SEM and confocal fluorescent images of L929 fibroblasts proliferated on the electrospun PG−HNT composite microfiber membranes with different halloysite contents (a, g) HNT0, (b, h) HNT1, (c, i) HNT2, (d, j) HNT5, (e, k) HNT 10, and (f, l) HNT20 for 5 days. The O.D. of L929 cells (m) adhered for 4 h and (n) proliferated for 1, 3, 5, and 7 days on the membranes tested using CCK-8 assay.

in the nanomicro fiber membrane was chosen 25 wt %: metronidazole incorporated directly in polymeric fibers was 20 wt % plus 5 wt % of metronidazole loaded in halloysite which provided the release time extension (25 wt % tube loading x 0.2 halloysite part = 5 wt %). The drug-loaded nanotubes were mixed with polycaprolactone−gelatin polymer (20 wt % HNT) for electrospinning formation of drug-loaded nanomicro fiber membranes (PG/HNT−MNA) where PG means polycaprolactone−gelatin matrix. Different composition of the membranes were fabricated, no halloysite−PG/MNA−20 wt % MNA; PG/HNT−MNA to polymer matrix in the fiber; and PG−MNA/HNT−MNA−20 wt % MNA, to compare the drug-release profile and biocompatibility of the membranes with direct drug loading, drug loading within halloysite nanotubes only, and mixed formulation. These different composition membranes were electrospun well with homogeneous fiber distribution. The addition of metronidazole and halloysite had no significant influence on the morphology of the membranes. The diameters of the nanofibers with different contents of drug were in the range of 300−400 nm (Figure S5, Supporting Information).

The release profiles of metronidazole from PG−MNA, PG/HNT−MNA, and PG−MNA/HNT−MNA are presented in Figure 9. The drug-release mechanism is based on the tube nanoconfined drug diffusion, slow diffusion through the fiber body, and polymer degradation and is based on two stages: nanopore-controlled diffusion from nanotubes and drug diffusion through the polymeric matrix. Though metronidazole releases from halloysite powders within 24 h, its incorporation into fibers drastically slows the process. Without halloysite, for PG−MNA, about 90% of the drug releases from the membrane within 4 days. After the initial burst, the metronidazole tends to release in a linear way in the following 2 days. With inclusion of drug-loaded halloysite nanotubes, such as PG/HNT−MNA sample, the drug shows a sustained 15-day release because metronidazole needs to be first released from the nanotubes to the polymer matrix and then through polymer to the medium. However, drug loading in this sample is ca. 5 wt %, which less than the allowed maximum.

The third formulation, combing the drug load both in microfiber body and in halloysite nanotubes, gave us the total load 20 + 5 = 25% with release kinetics representing combination of these two processes. For this PG−MNA/HNT−MNA sample, about 75 wt % MNA was released from the membrane within 4 days, and the remaining 25% released in a sustained manner for over 3 weeks due to the drug located inside the nanotubes. After 10 days, the drug released rate was still high enough to prevent the bacterial growth. We consider this formulation combining 5 wt % drug loading into the nanotubes with an additional 20 wt % load into the polymeric matrix as an essential improvement for the membrane antibacterial efficiency due to the release extended up to 3 weeks as compared with 4 days with no-halloysite formulation.

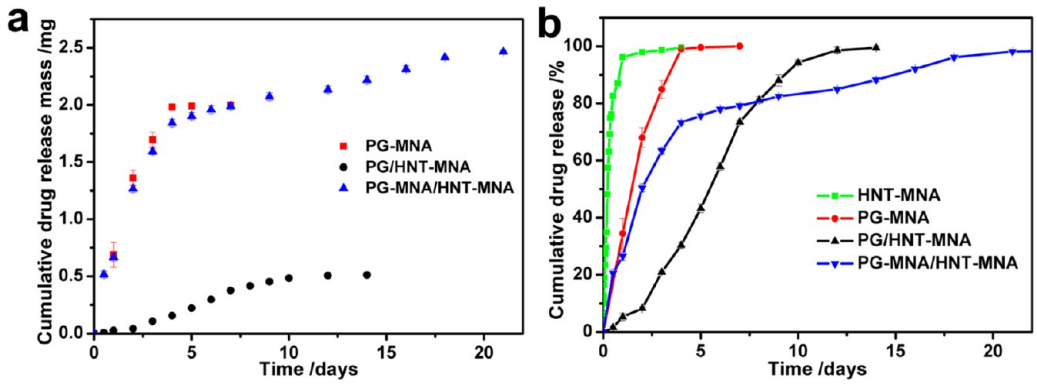

Figure 9. Cumulative drug release profiles: (a) released metronidazole (MNA) mass and (b) released percent for electrospun drug loaded membranes at different soaking times in PBS buffer.

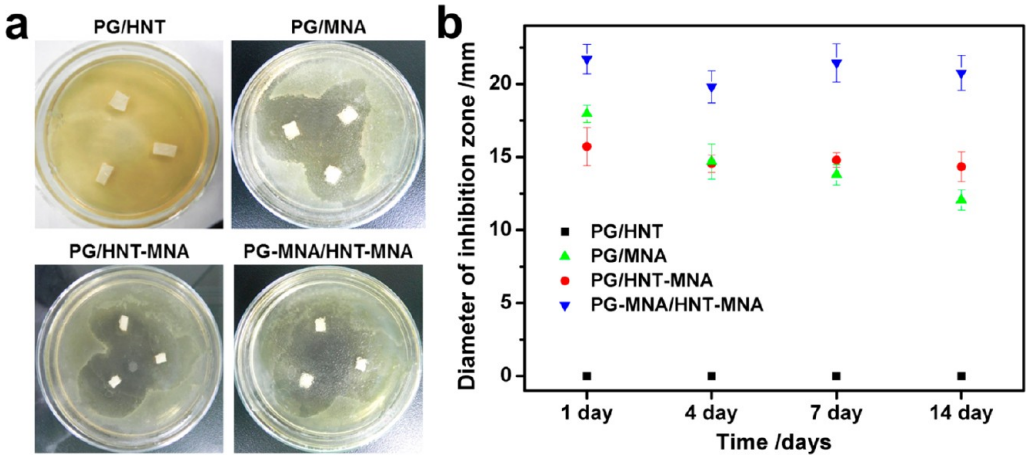

Figure 10. Inhibition of bacterial growth on agar plates of the drug-loaded nanomicro fiber membranes: (a) images of inhibition zone surrounding membranes after incubation for 1 day under anaerobic conditions at 37 °C; (b) inhibition zone diameter *versus* incubation time.

After the membrane is implanted into a tissue-defect site, the first week is the high-incidence period for infection and inflammation. Therefore, for the delivery of antibiotics, a high initial release rate in the first few days is best for eliminating the intruding bacteria. For the few bacteria that survive the initial burst, a continued drug release for 2 weeks is necessary to inhibit the occurrence of latent infection.[34] Therefore, the halloysite-based 3-week drug release profile could be an optimal treatment. The selected concentration of drug released at the tissue defect site is sufficiently high to inhibit the growth of bacteria but much lower than the systemic treatment dosage, and the halloysite concentration is also within the safe range (Figure S6, Supporting Information). During the infection, both aerobic and anaerobic bacteria present at the defect site. Different kind of drug with various functions could be loaded into halloysite clay nanotubes to realize multidrug cocktails with sustained and adjustable release profiles.

5. *In Vitro* Antibacterial Activity. The antibacterial activity of the drug-loaded membranes was evaluated using *Fusobacterium nucleatum* as a model anaerobic bacterium, which is commonly found in the oral cavity infections.[35] The growth of *F. nucleatum* can be visualized directly in a Petri dish (Figure 10). The inhibition zone diameters at different incubation time are presented in Figure 10b. Bacterial inhibition zones are clearly observed around drug-loaded PG/MNA, PG/HNT−MNA and PG−MNA/HNT−MNA, while no-drug PG/HNT sample did not show inhibition. The MNA loaded membranes inhibit bacterial growth in an area larger than the membrane size itself because of the drug diffusion into agar. From the inhibition zone diameter at different incubation time, at day one the inhibition zone of combined formulation PG−MNA/HNT−MNA is the largest. With the drug spread in larger volume, its potency decreases and the inhibition zone of PG−MNA decreases. But long-lasting drug release from nanotube composite PG−MNA/HNT−MNA keeps the inhibition zone around the membrane for a long time. This confirms that the encapsulation of metronidazole in the clay nanotubes has no adverse effect on the drug, and metronidazole released from halloysite fibers retains long-lasting antibacterial activity.

In vitro biocompatibility test of the drug loaded nanomicro composite: The viability of L929 mouse cells cultured in the extract substrates of the membranes

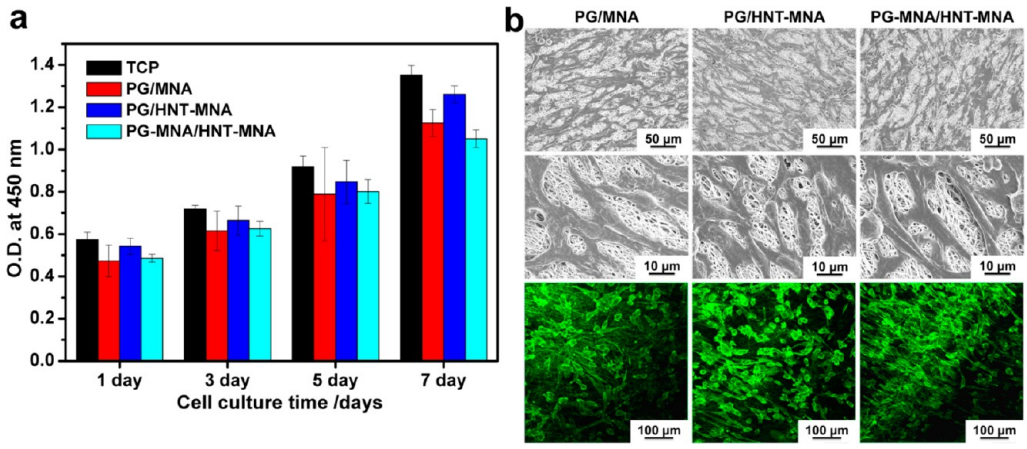

Figure 11. ***In vitro*** **biocompatibility of the electrospun drug-loaded nanomicro fiber membranes: (a) O.D. of L929 cells proliferated for 1, 3, 5, and 7 days on the membranes tested by using CCK-8 assay; (b) SEM micrographs and confocal fluorescent images of L929 fibroblasts proliferated on the membranes after 5 days.**

has no significant difference with that in the cell culture medium, reflecting that the MNA-loaded halloysite membranes show no cytotoxicity. The cells incubated for 72 h show spindle, triangular, and quadrangular shapes with good growing conditions (Figure S6, Supporting Information). Therefore, metronidazole loaded halloysite-fiber membranes show no cytotoxicity, while providing antimicrobial effect. The influence of drug on the biocompatibility of the membranes was also investigated by studying the viability of the cells proliferated. For all of the tested membranes, the number of cells increases continuously during 7 days of culture incubation, indicating that the membranes are nontoxic and support cell proliferation (Figure 11). As shown in SEM and CLSM micrographs, after 5 days of seeding, the cells reach 50−60% confluency with stretching shape and demonstrate extension and spreading cytoskeleton. The specific structures, filopodia and lamellipodia, related to the cell motility of fibroblasts was observed.

Therefore, even at high content of drugs, use of halloysite nanotubes and organic solvent during electrospinning, the "nano-in-micro" drug loaded membranes have no negative effect on cell viability and proliferation. Thus, this clay nanotube drug delivery system incorporated in electrospun microfibers could be used as an efficient anti-infection GTR/GBR membrane with a long-lasting drug release profile.

CONCLUSIONS

An efficient anti-infective GTR/GBR implant membrane made of drug-loaded clay nanotube doped electrospun polycaprolactone/gelatin microfibers was developed. Effective dispersion of the nanotubes in the electrospinning solution was reached by surface silanization. These 50 nm diameter and 600 nm length nanotubes were incorporated into the 400 nm diameter fibers resulting in the tube alignment and giving the membranes with anisotropic mechanical properties with twice the tensile strength along the collector rotating direction. Addition of 20 wt % of metronidazole−halloysite in the fibers allowed for 5 wt % drug loading in the membranes. By combining the drug-loading capability of the nanotubes and direct drug loading into electrospun microfiber matrix, composite membranes with 3-week sustained drug release were realized. Compared with conventional electrospun fiber-based drug delivery system, these nanomicro composite membranes have a smaller initial drug burst and increased release time. Comparing of our sustain drug delivery nanoformulation with, for example, polyelectrolyte nanoencapsuation[36] and LbL capsules and nanoshells,[37] one can underline a simplicity of our technique and much longer drug release time reaching 3−4 weeks. This extended release prevents the colonization of *Fusobacterium* over period of 3 weeks. The nanomicro fiber membranes are biocompatible and are exemplary GTR/GBR membranes. This inorganic−organic drug delivery membrane can be used in various therapeutic applications requiring time-extended functions, including pathologies demanding chronic drug treatments, wound healing, prevention of postsurgical adhesions, and tissue-engineering applications.

METHODS

Materials. PCL (M_n = 70−90 kDa) and 3-(4,5-dimethylthiazol-2-yl)-2,5-diphenyltetrazolium bromide (MTT) were purchased from Sigma-Aldrich (St. Louis, MO) and used as received. Gelatin was purchased from Rousselot (France). MNA was purchased from Tokyo Chemical Industry Co., Ltd. (Japan). Halloysite has been obtained from Applied Minerals Inc. Dulbecco's modified eagle medium (DMEM), fetal bovine serum (FBS), 0.05% Trypsin EDTA, and phosphate buffer saline (PBS, pH = 7.4) were

purchased from Gibco (USA). Methanol, APTES and trifluoroethanol were purchased from Alfa-Aesar Chemical, Inc. (USA). WST-8, polyformaldehyde and FITC−phalloidin were purchased from Beyotime Institute of Biotechnology (China). Other chemical reagents such as acetic acid, dichloromethane (DCM), and *N*,*N*′-dimethylformamide (DMF) were purchased from Sinopharm Chemical Reagent Beijing Co., Ltd. (China) and used without further purification. MGC AnaeroPack Series was purchased from Mitsubishi Gas Chemical Co., Inc. (Japan). Brain−heart infusion broth and brain−heart infusion agar were purchased form Oxoid (U.K.). L929 fibroblast cell lines were kindly donated by Jishuitan Hospital.

Modification of Halloysite. The surface of halloysite was modified with APTES to improve the dispersion of halloysite in the electrospinning solution of trifluoroethanol according to the procedure described previously.[19] APTES (500 μL) was dissolved in 6.25 mL of toluene, 0.15 g of halloysite powder was added, and the suspension was dispersed ultrasonically for 30 min. The suspension was then refluxed at 120 °C for 20 h under constant stirring. The resultant mixture was extensively washed with fresh toluene six times to remove the excess organosilane and then dried overnight at 120 °C for further curing. The mixture was then washed 10 times with deionized water, and the sample was freeze-dried overnight. The amino-functionalized halloysite could disperse homogeneously in the electrospinning solution for over 1 week without aggregation.

The internal structure of halloysite was analyzed with transmission electron microscopy (TEM, JEM-2100F) at 120 kV. The external surface morphologies and surface elemental compositions of halloysite before and after modification were characterized using a scanning electron microscope (Hitachi S4800 FE-SEM). FT-IR spectra of raw and modified halloysite were performed from 4000 to 600 cm^{-1} at 2 cm^{-1} resolution with a Bruker Tensor 27 spectrometer. Thermogravimetric (TGA) measurements were carried out on a STARe system TGA/DSC1 thermogravimeter (Mettler-Toledo International Inc., Switzerland). The samples were heated from 30 to 800 °C at a heating rate of 10 °C min^{-1}.

Cytotoxicity of the Modified Halloysite. MTT assay was used to test the cytotoxicity of the modified halloysite to L929 cells. The halloysite suspensions at different concentrations (1, 10, 100, and 1000 μg/mL) were diluted with complete cell culture medium. L929 cells were resuspended in DMEM supplemented with 10% (v/v) FBS at a density of 10^4 cells/mL, and 100 μL of cell resuspension solution was pipetted into 96-well micrometer plates. After incubation at 37 °C under 5% CO_2 atmosphere for 24 h, the medium was replaced by the previously prepared extracted dilutions, with the culture medium as blank control and DMSO as negative control. After 24, 48, and 72 h of incubation with the modified halloysite, the morphologies of the cells in the plate were observed by using an inverted phase contrast microscope (Olympus IX50-S8F2). The cells were treated with 20 μL/well MTT (5 mg/mL in PBS solution) and incubated for another 4 h at 37 °C in a humidified atmosphere of 5% of CO_2. Then the culture medium was removed, and 200 μL/well of DMSO was added to dissolve the formed formazan crystals. After the plate was shaken for 15 min, the optical density (O.D.) was read on a multiwell microplate reader at 630 nm. The cytotoxicity for each membrane was tested by six averages of extract substrate. The viability percentage was expressed as the relative growth rate (RGR) by the equation

$$\mathrm{RGR} = (\mathrm{O.D._{\cdot sample}} - \mathrm{O.D._{\cdot DMSO}})/(\mathrm{O.D._{\cdot blank\ control}} - \mathrm{O.D._{\cdot DMSO}}) \times 100\%$$

where $\mathrm{O.D._{\cdot sample}}$, $\mathrm{O.D._{\cdot DMSO}}$ and $\mathrm{O.D._{\cdot blank\ control}}$ are the O.D. of the cells incubated in sample, DMSO, and the blank control.

Electrospinning of the Fiber Membranes and Their Characterization. A polymer solution with a concentration of 6 wt % was prepared by dissolving PCL and gelatin in trifluoroethanol under magnetic stirring for 24 h at room temperature. Modified halloysite, in the range of 1−20 wt % of the polymer used, was added to the electrospinning solution and stirred homogeneously. The solution was fed at a rate of 2 mL/h by a syringe pump to the needle tip of a 20 mL syringe. Optimized high voltage (8−12 kV) was applied between the needle and the grounded collector, which was laid with aluminum foil at a rotating rate of 300 rpm. The needle was located at a distance of 20 cm from the ground collector. As HNT content is 30%, the electrospinning process was not stable, so the highest HNT loading content is 20% for electrospinning. The membranes with HNT contents of 0%, 1%, 2%, 5%, 10%, and 20% were labeled as HNT0, HNT1, HNT2, HNT5, HNT10, and HNT20, respectively.

The morphology of the nanofiber membranes was observed by SEM. The fiber diameter and pore size were measured by using the ImageJ software on SEM micrographs at 100 random locations. Transmission electron microscopy (TEM, JEM-2100F) was conducted to confirm the encapsulation and arrangement of halloysite in the nanofibers. TEM samples were prepared by placing the carbon-coated copper grids on the collector and directly depositing a thin layer of electrospun nanofibers onto the copper grids.

TGA measurements were carried out on a STARe system TGA/DSC1 thermogravimeter. The samples were heated from 30 to 800 °C at a heating rate of 10 °C min^{-1}. DSC measurements were performed with a Mettler-Toledo DSC instrument under nitrogen. The measurements were carried out at cooling and heating rates of 10 °C/min from −100 to +220 °C. FT-IR spectra were performed on a Bruker Tensor 27 spectrometer. The scan range was 4000−600 cm^{-1} with a resolution of 2 cm^{-1}. X-ray diffraction (XRD) studies were conducted on a Rigaku D/max-Ultima III X-ray diffractometer equipped with Cu−K α source (40 kV, 40 mA) in the range of 5−50° at a scan rate of 5°/min.

The tensile properties of the membranes at directions along and perpendicular to the collector rotating direction were evaluated by using a BOSE ElectroForce 3200 test instrument with a 50-N load cell at a crosshead speed of 5 mm/min at the ambient temperature of 25 °C. All samples were cut into rectangles with dimensions of 25 mm × 4 mm. Five samples were tested for each membrane. The samples were soaked in deionized water for 1 h before testing to get the tensile properties at the wet state of the membranes. The thicknesses of the samples were measured with a micrometer accuracy.

Hydrophilicity of the membranes was evaluated on the basis of the analysis of contact angles of water droplets on the membranes, which were measured by a SL200A-type contact angle analyzer (Solon (Shanghai) Technology Science Co., Ltd., China). Water droplets (3.0 μL) were dropped carefully onto the surface of the electrospun membranes, and the dynamic change of the water was recorded by a video.

***In Vitro* Biodegradation and Biocompatibility of the Membranes.** The membrane was cut into circular samples 2 cm in diameter, weighed, and soaked in 5 mL of PBS in 12-well plates at 37 °C. At predetermined time intervals, samples were rinsed with Milli-Q water, dried at 50 °C until the weight underwent no further changes, and then weighed. The sample weights were plotted against time to obtain the degradation profile of the membrane. The morphology of the membrane during degradation was measured by SEM.

The cytotoxicity of the membranes to L929 fibroblast cells was evaluated by MTT assay (see Figure S7, Supporting Information). The viabilities of L929 cells proliferated on the membranes were assessed by using CCK-8 assay according to the manufacturer's protocol. The membrane was cut into circles 2.5 cm in diameter, sterilized, and then fixed in the well of a 24-well plate by Cell-Crown. L929 cells were resuspended in DMEM supplemented with 10% FBS at a density of 4.0 × 10^4 cells/mL. Cell culture medium (800 μL) and cell resuspension (100 μL) were plated onto the sample carefully. Cells proliferated on the tissue culture plate (TCP) was regarded as control. Plates were incubated at 37 °C under 5% CO_2 atmosphere. The medium was changed every 2 days. At days 1, 3, 5, and 7 of culture, the sample was washed with PBS three times to remove the cells that did not attach to the membrane, and 100 μL of WST-8 (final dilution: 1:10), which can react with dehydrogenase in mitochondria to form a water-soluble formazan, was added onto the sample to test the live cells. Then 100 μL of supernatants was transferred into a 96-well plate for optical density (O.D.) measurements at 450 nm. The cell-cultured membrane was then washed with PBS three times, fixed with 3% glutaraldehyde at 4 °C for 2 h, soaked in 0.18 M sucrose

solutions at 4 °C for 2 h, dehydrated through a series of graded ethanol solutions, and lyophilized overnight. The morphologies of the cells on the membranes were observed by using SEM.

The morphologies of the cells were also observed using laser scanning confocal microscope (CLSM, Olympus, FV1000-IX81). After incubated for 5 days, the cell-cultured samples were washed twice with PBS, fixed with 4% polyformaldehyde for 10 min, and then stained with FITC–phalloidin solution (5 μg/mL) for 1 h. The samples were washed three times with PBS and visualized with CLSM. The CLSM images were obtained by focusing on the surface of the membranes as z-position.

The *in vitro* barrier function of the membranes to L929 cells as model cells was evaluated by an elegant method we designed as described previously.[38] Briefly, cells were added onto the sample, after incubation for 7 days, the other side of the membrane was observed by SEM to find out whether cells penetrated the membrane.

Drug Loading–Release Procedures. Saturated solutions of MNA in trifluoroethanol were mixed with a dry HNT powder. The solution was placed in a vacuum chamber for 30 min. Air bubbles were popped up from the HNT pores to allow for antiseptic to enter the lumens. After 30 min, the vacuum was stopped, and air was allowed into the chamber. The process was repeated twice for the most efficient loading. After loading, the samples were separated from the solution by centrifugation and washed with water to remove any unloaded drug. Loaded HNT was dried in an oven at 50 °C and milled to fine powder. The mass ratio of HNT to MNA was changed to get the highest drug loading efficiency.

MNA release experiments were conducted by stirring loaded HNT in 1 mL of trifluoroethanol. At predetermined time intervals, the supernatant was removed by centrifugation at 7000 rpm (2 min), and fresh trifluoroethanol was added. The collected supernatant was detected by high-performance liquid chromatography (HPLC) at λ_{max} = 310 nm. The amount of MNA was obtained from the calibration curve of MNA.

To get estimation of the full tube loading, 100 mg of HNT was dispersed in 50 mL of water and sonicated for 30 min (until all MNA was released). Then supernatant was separated by centrifugation at 5000 rpm (10 min), and the total amount of MNA was measured with HPLC.[16]

Electrospinning of Drug-Loaded Microfiber Membranes and Release Measurement. A polymer solution (PG solution) with a concentration of 6 wt % was prepared by dissolving PCL and gelatin in trifluoroethanol under magnetic stirring for 24 h at room temperature. Then four different kinds of electrospinning solution were prepared by adding 20 wt % relative to PG of (1) HNT, (2) MNA, (3) MNA-loaded HNT, and (4) MNA and MNA-loaded HNT into the PG solution. The electrospinning process was conducted as described above except that the electrospinning solution with drug-loaded HNT added was changed every 1 h. The electrospinning membranes with different composition were labeled as PG/HNT, PG/MNA, PG/HNT–MNA, and PG–MNA/HNT–MNA, respectively. The morphology of the drug-loaded nanofiber membranes was observed by SEM.

The drug-release profile was determined by soaking the membrane in triplicate in PBS. The membrane was cut into circles 2 cm in diameter, accurately weighed, and incubated in 5 mL of PBS at 37 °C with mild shaking. At predetermined time intervals, 1 mL of soaking solution was collected for HPLC detection to determine the amount of drug released. The remaining medium was removed and replaced with another 5 mL of fresh PBS to maintain the sink conditions. The percentage of the drug released was calculated on the basis of the initial weight of the drug incorporated in the electrospun membrane.

***In Vitro* Antibacterial Activity and Cytotoxicity of Drug-Loaded Membranes.** The antibacterial activity of the membranes against the typical anaerobic bacterium *F. nucleatum* (ATCC 25586, Chinese General Microbiological Culture Collection Center), which is commonly found in the oral cavity in an infection,[35] was determined by the modified Kirby–Bauer method under anaerobic conditions as previous desribed.[11] A 100 μL *F. nucleatum* suspension was spread onto a brain–heart infusion agar plate. Samples (1.0 cm × 1.0 cm) of a membrane in triplicate were sterilized, pasted onto the agar plate, and then incubated anaerobically with a MGC AnaeroPack-Anaero Series for different times at 37 °C. The bacterial growth on the plate was visualized directly, and the diameter of the inhibition zone was measured within 2 weeks.

The cytotoxicity of the membranes to L929 fibroblast cells was detected by MTT assay, and the proliferation of cells on the membranes was assessed by using CCK-8 assay, similar to above-described procedures of the characterization methods of the *in vitro* biocompatibility of the HNT-doped nanofiber membranes.

Conflict of Interest: The authors declare no competing financial interest.

Supporting Information Available: Details on cytotoxicity of the halloysite nanotubes, the biodegradation and the barrier function of the halloysite nanomicro fiber membranes, release of the drug from halloysite nanotubes, SEM morphology of the drug-loaded nanofiber membranes, calculation of the concentration of MNA and HNT at the defect site, cytotoxicity of the drug loaded nanofiber membranes, and the cytotoxicity evaluation of the HNT-doped electrospun microfiber membranes. This material is available free of charge *via* the Internet at http://pubs.acs.org.

Acknowledgment. This work was supported by the National Natural Science Foundation of China (50933001, 51221102, 81171682, 81330043, and 51303014), Beijing Nova Program (Z131102000413015). Chinese Ministry of Education – "Distinguished Overseas Scholar Project".

REFERENCES AND NOTES

1. Karring, T.; Nyman, S.; Lindhe, J. Healing Following Implantation of Periodontitis Affected Roots into Bone Tissue. *J. Clin. Periodontol.* **1980**, *7*, 96–105.
2. Gentile, P.; Chiono, V.; Tonda-Turo, C.; Ferreira, A. M.; Ciardelli, G. Polymeric Membranes for Guided Bone Regeneration. *Biotechnol. J.* **2011**, *6*, 1187–1197.
3. Retzepi, M.; Donos, N. Guided Bone Regeneration: Biological Principle and Therapeutic Applications. *Clin. Oral Implants Res.* **2010**, *21*, 567–576.
4. Ragel, C.; Vallet-Regi, M. *In Vitro* Bioactivity and Gentamicin Release from Glass-Polymer-Antibiotic Composites. *J. Biomed. Mater. Res.* **2000**, *51*, 424–429.
5. Campoccia, D.; Montanaro, L.; Arciola, C. A Review of the Clinical Implications of Anti-Infective Biomaterials and Infection-Resistant Surfaces. *Biomaterials* **2013**, *34*, 8018–8029.
6. Feng, K.; Sun, H.; Bradley, M.; Dupler, E.; Giannobile, W.; Ma, P. Novel Antibacterial Nanofibrous PLLA Scaffolds. *J. Controlled Release* **2010**, *146*, 363–369.
7. Bottino, M.; Thomas, V.; Schmidt, G.; Vohra, Y. K.; Chu, T.; Kowolik, M.; Janowski, G. Recent Advances in the Development of GTR/GBR Membranes for Periodontal Regeneration—A Materials Perspective. *Dent. Mater.* **2012**, *28*, 703–721.
8. Lofmark, S.; Edlund, C.; Nord, C. Metronidazole Is Still the Drug of Choice for Treatment of Anaerobic Infections. *Clin. Infect. Dis.* **2010**, *50* (Suppl 1), S16–23.
9. Sill, T. J.; von Recum, H. A. Electrospinning: Applications in Drug Delivery and Tissue Engineering. *Biomaterials* **2008**, *29*, 1989–2006.
10. Liu, W.; Thomopoulos, S.; Xia, Y. Electrospun Nanofibers for Regenerative Medicine. *Adv. Healthcare Mater.* **2012**, *1*, 10–25.
11. Xue, J.; He, M.; Liu, H.; Niu, Y.; Crawford, A.; Coates, P. D.; Chen, D.; Shi, R.; Zhang, L. Drug Loaded Homogeneous Electrospun PCL/Gelatin Hybrid Nanofiber Structures for Anti-Infective Tissue Regeneration Membranes. *Biomaterials* **2014**, *35*, 9395–9405.
12. Hu, C.; Liu, S.; Zhang, Y.; Li, B.; Yang, H.; Fan, C.; Cui, W. Long-Term Drug Release from Electrospun Fibers for *In Vitro* Inflammation Prevention in the Prevention of Peritendinous Adhesions. *Acta Biomater.* **2013**, *9*, 7381–7388.

13. Beck-Broichsitter, M.; Thieme, M.; Nguyen, J.; Schmehl, T.; Gessler, T.; Seeger, W.; Agarwal, S.; Greiner, A.; Kissel, T. Novel "Nano in Nano" Composites for Sustained Drug Delivery: Biodegradable Nanoparticles Encapsulated into Nanofiber Non-Wovens. *Macromol. Biosci.* **2010**, *10*, 1527–1535.
14. Zhang, C. L.; Yu, S. H. Nanoparticles Meet Electrospinning: Recent Advances and Future Prospects. *Chem. Soc. Rev.* **2014**, *43*, 4423–4448.
15. Wei, W.; Abdullayev, E.; Hollister, A.; Mills, D.; Lvov, Y. M. Clay Nanotube/Poly(methyl methacrylate) Bone Cement Composites with Sustained Antibiotic Release. *Macromol. Mater. Eng.* **2012**, *297*, 645–653.
16. Veerabadran, N.; Price, R.; Lvov, Y. Clay Nanotubes for Encapsulation and Sustained Release of Drugs. *Nano* **2007**, *02*, 115–120.
17. Lvov, Y.; Abdullayev, E. Functional Polymer–Clay Nanotube Composites with Sustained Release of Chemical Agents. *Prog. Polym. Sci.* **2013**, *38*, 1690–1719.
18. Du, M.; Guo, B.; Jia, D. Newly Emerging Applications of Halloysite Nanotubes: a Review. *Polymer Int.* **2010**, *59*, 574–595.
19. Vergaro, V.; Abdullayev, E.; Lvov, Y.; Zeitoun, A.; Cingolani, R.; Rinaldi, R.; Leporatti, S. Cytocompatibility and Uptake of Halloysite Clay Nanotubes. *Biomacromolecules* **2010**, *11*, 820–826.
20. Zhang, Y.; Gao, R.; Liu, M.; Yan, C.; Shan, A. Adsorption of Modified Halloysite Nanotubes *In Vitro* and the Protective Effect in Rats Exposed to Zearalenone. *Arch. Anim. Nutr.* **2014**, *68*, 320–335.
21. Lvov, Y.; Shchukin, D.; Möhwald, H.; Price, R. Halloysite Clay Nanotubes for Controlled Release of Protective Agents. *ACS Nano* **2008**, *2*, 814–820.
22. Qi, R.; Guo, R.; Shen, M.; Cao, X.; Zhang, L.; Xu, J.; Yu, J.; Shi, X. Electrospun Poly(lactic-co-glycolic acid)/Halloysite Nanotube Composite Nanofibers for Drug Encapsulation and Sustained Release. *J. Mater. Chem.* **2010**, *20*, 10622–10629.
23. Qi, R.; Guo, R.; Zheng, F.; Liu, H.; Yu, J.; Shi, X. Controlled Release and Antibacterial Activity of Antibiotic-Loaded Electrospun Halloysite/Poly(lactic-co-glycolic acid) Composite Nanofibers. *Colloids Surf., B* **2013**, *110*, 148–155.
24. Zhang, J.; Zhang, Y.; Chen, Y.; Du, L.; Zhang, B.; Zhang, H.; Liu, J.; Wang, K. Preparation and Characterization of Novel Polyethersulfone Hybrid Ultrafiltration Membranes Bending with Modified Halloysite Nanotubes Loaded with Silver Nanoparticles. *Ind. Eng. Chem. Res.* **2012**, *51*, 3081–3090.
25. Chao, C.; Liu, J.; Wang, J.; Zhang, Y.; Zhang, B.; Zhang, Y.; Xiang, X.; Chen, R. Surface Modification of Halloysite Nanotubes with Dopamine for Enzyme Immobilization. *ACS Appl. Mater. Interfaces* **2013**, *5*, 10559–10564.
26. Catledge, S. A.; Clem, W. C.; Shrikishen, N.; Chowdhury, S.; Stanishevsky, A. V.; Koopman, M.; Vohra, Y. K. An Electrospun Triphasic Nanofibrous Scaffold for Bone Tissue Engineering. *Biomed. Mater. (Bristol, U.K.)* **2007**, *2*, 142–150.
27. Richard-Lacroix, M.; Pellerin, C. Molecular Orientation in Electrospun Fibers: From Mats to Single Fibers. *Macromolecules* **2013**, *46*, 9473–9493.
28. Li, J.; Zuo, Y.; Cheng, X.; Yang, W.; Wang, H.; Li, Y. Preparation and Characterization of Nano-Hydroxyapatite/Polyamide 66 Composite GBR Membrane with Asymmetric Porous Structure. *J. Mater. Sci. Mater. Med.* **2009**, *20*, 1031–1038.
29. Dobrovolskaia, M. A.; McNeil, S. E. Immunological Properties of Engineered Nanomaterials. *Nat. Nanotechnol.* **2007**, *2*, 469–478.
30. Goddard, J. M.; Hotchkiss, J. H. Polymer Surface Modification for the Attachment of Bioactive Compounds. *Prog. Polym. Sci.* **2007**, *32*, 698–725.
31. Sculean, A.; Nikolidakis, D.; Schwarz, F. Regeneration of Periodontal Tissues: Combinations of Barrier Membranes and Grafting Materials - Biological Foundation and Preclinical Evidence: a Systematic Review. *J. Clin. Periodontol.* **2008**, *35*, 106–116.
32. Ji, W.; Yang, F.; Seyednejad, H.; Chen, Z.; Hennink, W. E.; Anderson, J. M.; van den Beucken, J. J.; Jansen, J. A. Biocompatibility and Degradation Characteristics of PLGA-Based Electrospun Nanofibrous Scaffolds with Nanoapatite Incorporation. *Biomaterials* **2012**, *33*, 6604–6614.
33. Peppas, N. A. Analysis of Fickian and Non-Fickian Drug Release from Polymers. *Pharm. Acta Helv.* **1985**, *60*, 110–111.
34. Kim, K.; Luu, Y. K.; Chang, C.; Fang, D.; Hsiao, B. S.; Chu, B.; Hadjiargyrou, M. Incorporation and Controlled Release of a Hydrophilic Antibiotic Using Poly(lactide-co-glycolide)-Based Electrospun Nanofibrous Scaffolds. *J. Controlled Release* **2004**, *98*, 47–56.
35. Signat, B.; Roques, C.; Poulet, P.; Duffaut, D. Fusobacterium Nucleatum in Periodontal Health and Disease. *Curr. Issues Mol. Biol.* **2011**, *13*, 25–36.
36. Antipina, M.; Sukhorukov, G. Remote Control Over Guidance and Release Properties of Composite Polyelectrolyte Based Capsules. *Adv. Drug Del. Rev.* **2011**, *63*, 716–729.
37. Delcea, M.; Möhwald, H.; Skirtach, A. Stimuli-responsive LbL capsules and nanoshells for drug delivery. *Adv. Drug Del. Rev.* **2011**, *63*, 716–729.
38. Xue, J.; He, M.; Liang, Y.; Crawford, A.; Coates, P.; Chen, D.; Shi, R.; Zhang, L. Fabrication and Evaluation of Electrospun PCL-Gelatin Micro-/Nanofiber Membranes for Anti-Infective GTR Implants. *J. Mater. Chem. B* **2014**, *2*, 6867–6877.